iScience

CellPress

Article

Printable Metal-Polymer Conductors for Highly Stretchable Bio-Devices

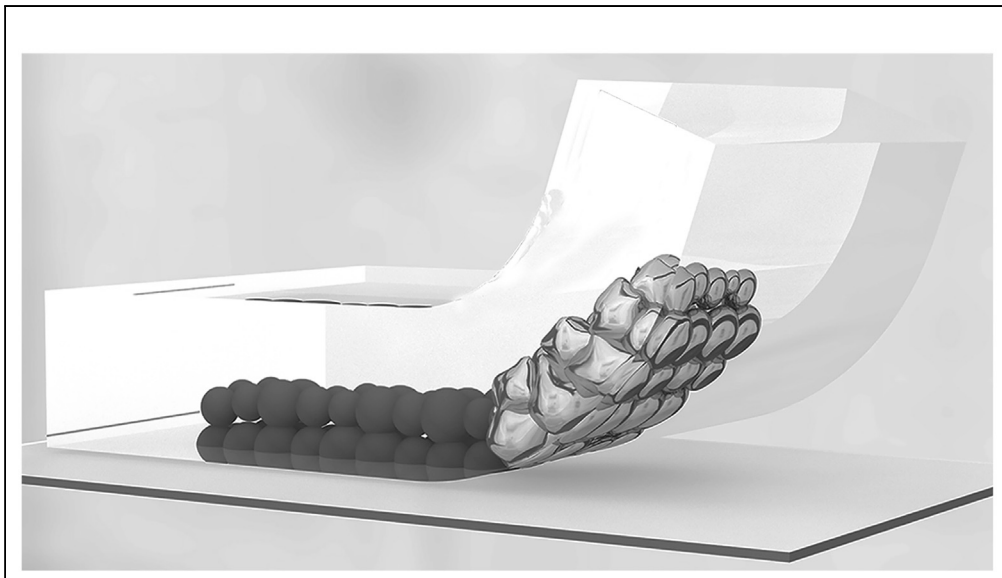

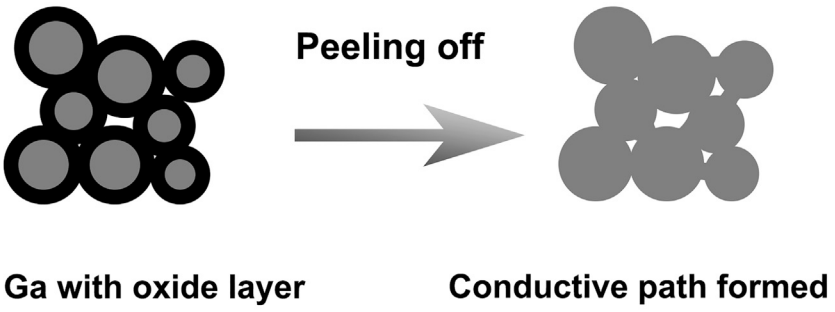

Lixue Tang, Shiyu Cheng, Luyao Zhang, ..., Zhiwei Huang, Xinghua Shi, Xingyu Jiang

xingyujiang@nanoctr.cn

HIGHLIGHTS

A straightforward method for sintering liquid metal particles with high efficiency

Liquid metal can be patterned on different substrates with high resolution

Low-cost, high-throughput, stretchable printed conductors can be fabricated

Conductors are biocompatible and have potentials in implantable electronics

Tang et al., iScience 4, 302–311
June 29, 2018
https://doi.org/10.1016/j.isci.2018.05.013

iScience

CellPress

Article

Printable Metal-Polymer Conductors for Highly Stretchable Bio-Devices

Lixue Tang,[1,2] Shiyu Cheng,[1,2] Luyao Zhang,[1,2,3] Hanbing Mi,[1,2] Lei Mou,[1,2] Shuaijian Yang,[2] Zhiwei Huang,[2] Xinghua Shi,[1,2] and Xingyu Jiang[1,2,4,*]

SUMMARY

Stretchable, biocompatible devices can bridge electronics and biology. However, most stretchable conductors for such devices are toxic, costly, and regularly break/degrade after several large deformations. Here we show printable, highly stretchable, and biocompatible metal-polymer conductors by casting and peeling off polymers from patterned liquid metal particles, forming surface-embedded metal in polymeric hosts. Our printable conductors present good stretchability (2,316 S/cm at a strain of 500%) and repeatability ($\Delta R/R$ <3% after 10,000 cycles), which can satisfy most electrical applications in extreme deformations. This strategy not only overcomes large surface tension of liquid metal but also avoids the undesirable sintering of its particles by stress in deformations, such that stretchable conductors can form on various substrates with high resolution (15 μm), high throughput (~2,000 samples/hour), and low cost (one-quarter price of silver). We use these conductors for stretchable circuits, motion sensors, wearable glove keyboards, and electroporation of live cells.

INTRODUCTION

Fusion of electronics with biology and medicine demands electronic devices that are supple, stretchable, and compatible with human tissues, such as the skin (Kim et al., 2011; Oh et al., 2016) and the brain (Kang et al., 2016; Liu et al., 2015), especially in the fields of health monitoring and disease treatment (Chortos et al., 2016; Sun et al., 2014; Jeong et al., 2015a). Flexible circuits are currently realized by depositing a thin layer of metal like copper and gold on flexible substrates such as polyimide. To further endow such flexible circuits with stretchability, wavy or serpentine structures are designed to counteract deformations (Lou et al., 2017; Kim et al., 2008). The stretchability of these strategies is limited (about 150%), and the fabrication processes of such structures are often complicated. Another approach is developing conductive materials that could bear large deformations such as carbon nanomaterials, silver inks, and liquid metals (LMs) (Kazem et al., 2017; Qi et al., 2015; Zheng et al., 2014; Matsuhisa et al., 2017; Tang et al., 2014). Most of these materials are hard to be patterned with microstructures in large scale. Among these materials, LMs, especially eutectic gallium indium alloy (EGaIn, melting point 15°C), stand out for their excellent performances of high conductivity and unequaled stretchability (Dickey, 2017). Besides, EGaIn is much less toxic (Lu et al., 2015) than other metals that may potentially be useful for these applications, such as mercury (also liquid at room temperature) or silver (its nanowires can withstand stretch). However, the huge surface tension (>400 mN/m) (Dickey, 2014) of LM impedes its direct patterning by using straightforward technologies such as stencil and ink-jet printing (Zheng et al., 2014; Wang et al., 2015), making its patterning limited to very few substrates that can be wetted by LMs. In addition, such strategies have high LM consumption (the thickness of the LM pattern is usually larger than 100 μm), which further limits their wider applications. Another common method, injecting the LM into microfluidic channels or hollow wires, can yield conductors with high stretchability (>1,000%). However, these methods cannot fabricate complex conductive patterns that require the microfluidic channels or hollow wires to be continuous from the beginning to end (Kubo et al., 2010; Zhu et al., 2013). By contrast, bottom-up approaches to fabricate LM into particles is a good way to minimize the surface tension. Some reported strategies usually deposit a layer of liquid metal particles (LMPs) (not conductive due to the oxide layer on the particles) on the surface of elastomers and use a marker to mechanically sinter LMPs (break the oxide layer to release the conductive LM) to obtain a desirable conductive pattern (Lin et al., 2015; Boley et al., 2015; Ren et al., 2016; Mohammed and Kramer, 2017). However, conductive patterns fabricated by these strategies cannot bear large deformations like stretching in practical applications, because stress in deformations will also sinter the LMPs in regions where conductive patterns are not desirable, causing short circuit in the electronics. Besides, using a marker to sinter the LMP to obtain electronics has low efficiency and low utilization of particles. These strategies using LMPs are not applicable to mass-manufacturing.

[1]Beijing Engineering Research Center for BioNanotechnology and CAS Key Laboratory for Biomedical Effects of Nanomaterials and Nanosafety, CAS Center for Excellence in Nanoscience, National Center for NanoScience and Technology, No. 11 Zhongguancun Beiyitiao, Beijing 100190, P. R. China

[2]University of Chinese Academy of Sciences, 19 A Yuquan Road, Shijingshan District, Beijing 100049, P. R. China

[3]State Key Laboratory of Nonlinear Mechanics, Institute of Mechanics, Chinese Academy of Sciences, Beijing 100190, P. R. China

[4]Lead Contact

*Correspondence: xingyujiang@nanoctr.cn

https://doi.org/10.1016/j.isci.2018.05.013

Here, we report printable and mass-manufacturable metal-polymer conductors (MPCs) by fabricating LM into LMPs (liquid core-oxide shell structure), and embedding the patterned LMPs on the surface of polymers by casting and peeling off steps, instead of using a marker or a nozzle, to result in microstructured, conductive path. The theoretical calculation indicates that the stress on the particles during stripping is much larger than the yield stress of gallium oxide, causing the release of the LM to form conductive paths. We used screen printing or microfluidic patterning strategy to pattern any 2D MPC pattern on various substrates in different thicknesses with high resolution (15 μm), high efficiency, and low cost. The printable MPC is highly conductive (8×10^3 S/cm), robust, and stretchable, which can keep conductivity as high as 2,316 S/cm at a strain of 500%. Because MPC patterns allow exposed LMs on the surface of polymer substrates (instead of completely buried within polymers), electronic components could be easily mounted. We used the printable MPC for highly stretchable circuits, motion sensors, wearable glove keyboards, and electroporation of live cells because of its biocompatibility. This potentially widely applicable approach will greatly increase the stretchability of electronic devices and sharply decrease the production cost of printed electronics, which will significantly promote the development of wearable or implantable electronic devices.

RESULTS

Fabrication of the MPC

To prove that the stress during stripping can effectively break the oxide layer of LMPs embedded in elastomers, we performed a theoretical calculation. We analyzed the stress of LMPs on the bending part (Figure 1A). The model can be simplified as a gallium particle embedded in a PDMS (polydimethylsiloxane) matrix. Through calculation, we concluded that the maximum Tresca's equivalent stress on the oxide layer of the particle is $\sigma_{max} = 5RE_m\varepsilon/2t = 4500$ MPa (E_m, ε, R, and t are the Young's modulus, strain at the bottom of the PDMS, the average radius of particles, and the thickness of gallium oxide, respectively), which is much larger than the yield stress of gallium oxide, σ_y = 200 MPa (details of calculation are shown in Figure S1, and mechanical calculation in Transparent Methods). It suggests that upon peeling off the PDMS from the LMP-patterned substrates, the oxide layer of the LM will yield and release the conductive core to form conductive paths.

Based on this mechanism, we developed an MPC micro-patterning strategy (Figure 1B). To prepare the LMP inks, we added LM (here we used EGaIn) into an organic, volatile solvent (n-decyl alcohol) and sonicated the mixture to convert EGaIn to LMP-based inks. The sonicated LMs tend to be particles with spherical shape, due to their large surface tension, thus the most straightforward way to pattern them would be to use 0D LMs rather than 1D wires or tubes. The diameters of the particles depend on the sonication time (Figure S2A). LMPs dispersed in solvent will not be sintered by stress. However, after the volatilization of the solvent, LMPs in ink become very sensitive to stress and any disturbance by the blade during printing will sinter the LMPs together. To increase the operation time for printing, we choose solvents with high boiling point instead of the commonly used ethanol. The n-decyl alcohol has higher boiling point (232.9°C) and more appropriate viscosity, allowing sufficient operation time for printing. We tested the viscosity and the contact angle of the LMP inks with different concentrations (Figures S2B and S2C). The LMP inks have contact angle in polyethylene terephthalate (PET) film smaller than 30° and viscosity around 20,000 cP. After printing of LMPs on the initial patterning layer (IPL) and evaporation of the solvent, the LMPs are stacked one atop another on the IPL (Figure 2A). At this point, the oxide layer of each particle inhibits electrical conductivity. We cast curable pre-polymers onto the stacked particles as the stripping layer (SL). Because our LMPs (about 5 μm in diameter) are in tight contact with each other and have larger density than polymers, the polymer cannot push neighboring LMPs apart. After curing the polymer and peeling it off, the tensile stress will break the oxide layer, forming pathways for electron transport; we can thus obtain microstructured MPC surface embedded on the IPL and/or SL (Figure 1A).

Characterization of the MPC

We characterized the structure of the MPC. MPC is composed of interlinked LM and infiltrated, porous polymeric host (Figure 1). The surface of MPC presented an "islands-in-the-sea" appearance, as LM islands are dispersed in the sea of polymers when using a variety of curable polymers with a broad range of hardness/elasticity (modulus from 30 kPa to 5 GPa) as the SL (Figures 2B and S3A). To confirm that the metallic phase within the MPC is interlinked, we exposed the MPC to a sulfuric acid solution, which will dissolve the LM but not the polymer, to see if the LM within the MPC can dissolve completely. The continuous hollow space left in the cross section of MPC after sulfuric acid treatment suggests that the LM must have formed a

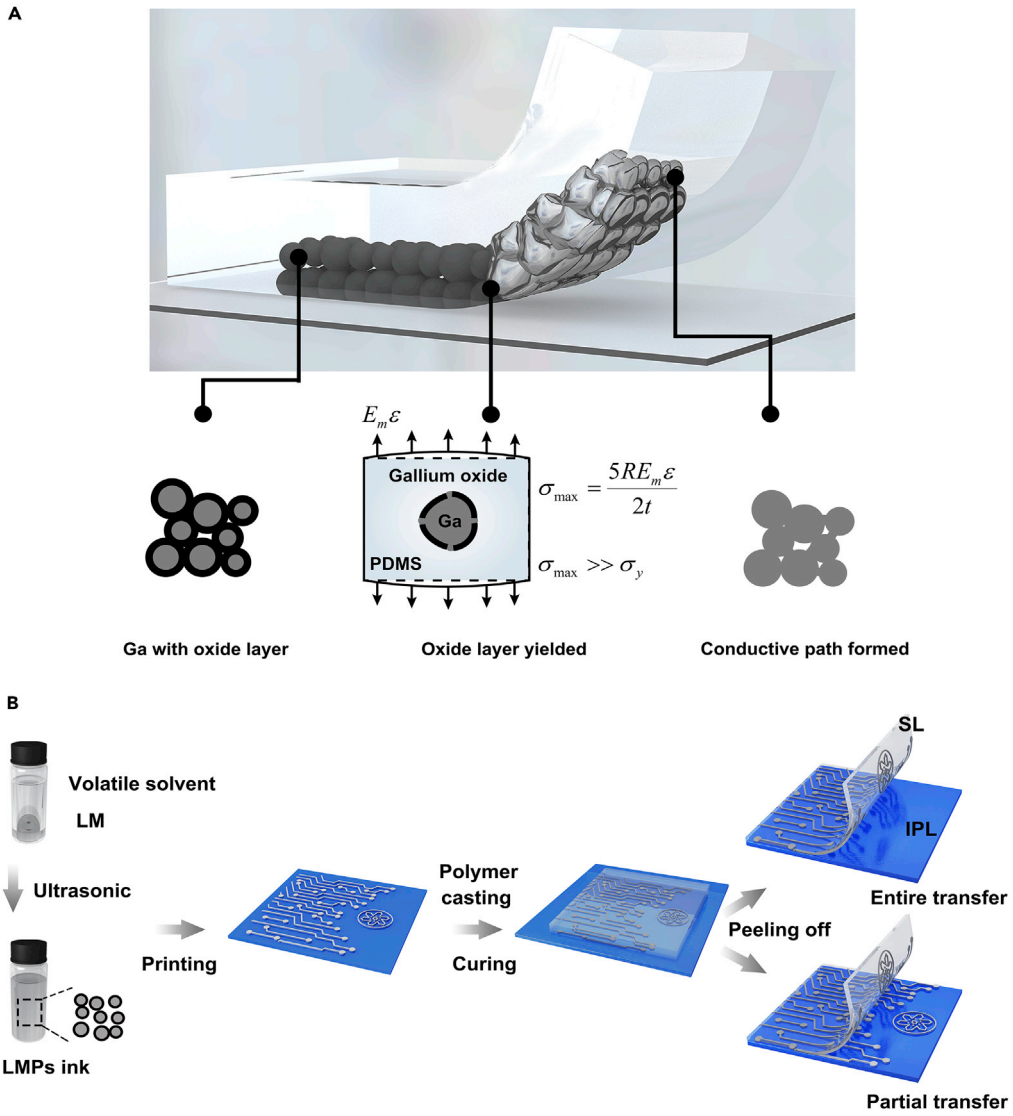

Figure 1. Conductive Mechanism and Fabrication of the MPC

(A) The oxide layer of LMPs will yield and form conductive paths after peeling off PDMS from the LMP-patterned substrate. σ_{max} is the maximum Tresca's equivalent stress on the oxide layer of the particle, σ_y represents yield stress of gallium oxide, and E_m,ε, R, and t are the Young's modulus, strain at the back end of the PDMS, the average radius of particles, and the thickness of gallium oxide, respectively.

(B) Fabricating microstructured MPC.

See also Figures S1 and S2, and Table S1.

continuous phase within the MPC; if the LM did not form a continuous phase, we would not expect the sulfuric acid to dissolve the LM in the middle of the MPC (Figure 2C). The continuous LM inside the MPC ensures unparalleled conductivity, while the LM islands on the surface promise stable contact with external devices. Unlike the LM surfaces, the MPC will not stick to the operator's finger upon gentle touch. Also, after connecting other devices with our MPC interconnects, we can use another layer of polymer to completely encase the MPC to avoid damage by sharp objects. MPCs cast by different polymers have similar conductivities (about 8×10^3 S/cm, Figure S2D). In comparison, without the stripping step, an MPC of similar size appears as an insulator. Both morphological and electrical analyses indicate that MPC has a continuous phase of conductive material embedded within the polymeric host.

We evaluated the electro-mechanical properties of the MPC cast by elastic polymer Ecoflex 0030 (a commercial silicone softer than PDMS). This MPC has a high initial conductivity (8×10^3 S/cm) and an excellent

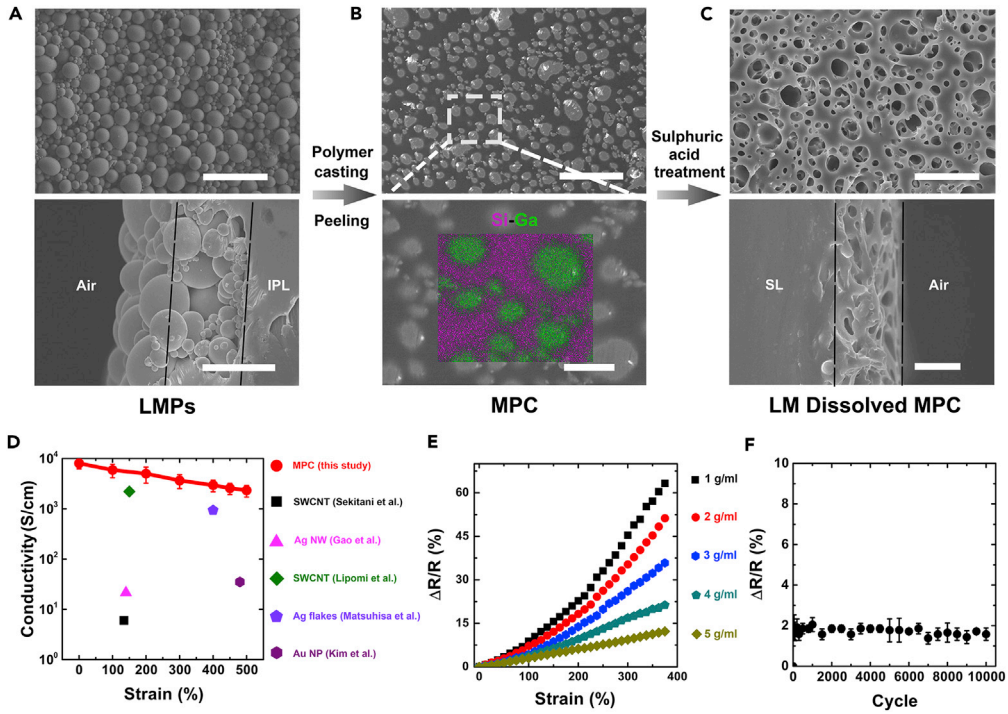

Figure 2. Characterization of the MPC

(A) Scanning electron microscopy of LMPs: *top*, top view; *bottom*, cross-sectional view. Scale bar, *top*, 30 μm; *bottom*, 10 μm. Black dashed line: region of stacked LMPs.

(B) The scanning electron microscopic and elemental analyses of the surface of the MPC. LM islands (green: Ga) in the sea of polymer (purple: Si). Scale bar, *top*, 30 μm; *bottom*, 5 μm.

(C) The MPC after dissolving the LM. *Top*, surface appearance, scale bar, 20 μm; *bottom*, cross-sectional appearance, scale bar, 10 μm. Dashed line: thickness of the MPC.

(D) Conductivity dependence on tensile strain of printed MPC and comparison with reported printed conductors.

(E) The change of resistance with different strain using MPC patterns printed by inks with different concentrations.

(F) ΔR/R changes with a strain of 50% for 10,000 cycles. Data in (D) and (F) are expressed as mean ± SD.

See also Figures S3 and S4.

stretchability, retaining a conductivity of 2,316 S/cm at a strain of 500%, which is comparable to those of stretchable, printed conductors under similar strains reported so far (Figure 2D) (Matsuhisa et al., 2017; Kim et al., 2013; Sekitani et al., 2009; Gao et al., 2014; Lipomi et al., 2011). We did not push the limit of stretchability further because an extension of 500% can itself satisfy the requirements of all our applications. To verify the performance of the MPC connected to a device, we used EGaIn as solder to weld a 100-Ω resistor to the MPC interconnects screen printed by different concentrations of LMP inks. The change of resistance of the MPC can be precisely tuned by inks with different concentrations of LMPs (Figure 2E). To test the repeatability of stretch, we repeatedly exerted tensile strain to an MPC strip (2.5 g/mL) cast by PDMS for 10,000 cycles (Figure 2F), the resistance kept essentially the same: ΔR/R <3% after 10,000 cycles. After the peeling off of the polymers, most of the particles are broken, forming a stable conductive structure; we thus do not see any change in resistance after the strain cycle. We characterized the MPC after 10,000 stretch cycles: several LM droplets with diameters of hundreds of micrometers will be squeezed out from several LM "islands" on the surface of MPC (Figure S4). However, the squeezed LMs cause no problem with regard to the electrical performance of the MPC (Figure 2F). The leakage of the LM can be prevented by encapsulating another layer of polymer on the surface of MPC.

Patterning of the MPC

To show that the MPC allows patterning of microstructured conductor on non-cured materials such as PET, glass, and paper using these substrates as the IPL, we try to decrease the amount of LM transferred onto the SL, since we have already achieved MPC patterning on different SLs such as PLGA [poly (DL-lactide-co-glycolide)] and PCL [poly (caprolactone)] by casting different polymers (Figure S6 top). Entire transfer

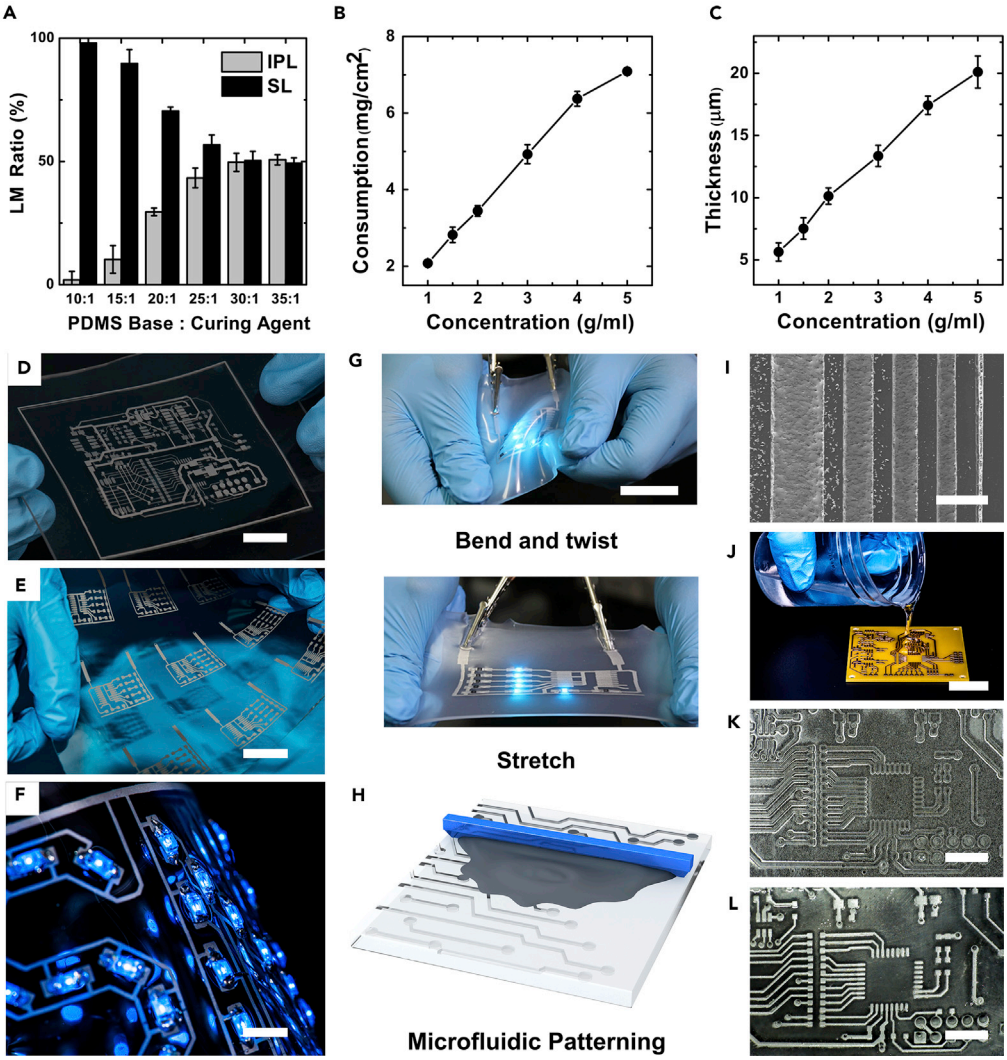

Figure 3. Micro-patterning of the MPC

(A) Transfer amount of LM versus different concentration of curing agent in PDMS.

(B) The consumption of LM versus the concentration of LMP inks.

(C) The thickness of the LMP patterns versus the concentration of LMP inks.

(D) A mutilayered circuit by stacking MPC patterned on pieces of PDMS.

(E) Large-scale production of circuit arrays by screen printing.

(F) An LED array.

(G) An LED circuit deformed by bending, twisting, and stretching.

(H) A schematic to demonstrate the microfluidic patterning method.

(I) MPC-filled ultrafine channels.

(J–L) Process of the microfluidic patterning using a PBC board as a convex mold. (J) PDMS casting, (K) PDMS replica, (L) MPC-filled microfluidic channels as a stretchable circuit. Scale bars: (D) 15 mm, (E) 3 cm, (F, K, and L) 5 mm, (G and J) 2 cm, and (I) 200 μm. Data in (A), (B), and (C) are expressed as mean ± SD.

See also Figures S5–S7, and Video S1.

(Figure S5A) or partial transfer (Figure S5B) mainly depends on the affinity between the IPL and the SL. Compared with the polymer, the structure of MPC (a porous structure of polymer with LM filled in the porous) is fragile and can be torn apart in the Z direction (Figure S5B bottom), such that part of the MPC becomes attached to the IPL if the affinity between the IPL and the polymer in the SL is large enough. Since increasing the base-to-curing-agent ratio for PDMS can increase its stickiness, we used PDMS with different proportion of curing agent as the SL (PET as the IPL) to control the transfer amount of LM. When this ratio exceeds 30:1, IPL can retain the maximum amount of LM (50%) (Figure 3A), such that complete 2D patterns

formed on both IPL and SL. To keep the feature resolution intact on SL, we need to decrease the affinity between the IPL and SL. To keep the feature resolution intact on IPL, we need to increase such affinity. The surface in partial transfer reflects the inner structure of the MPC, which presents a continuous metallic phase (Figure S3B). This strategy allows further broadening of the types of substrates on which we can pattern flexible microstructured conductors. For instance, when using non-curable materials (Figure S6 bottom) as the IPL, they can keep the MPC patterns by using sticky PDMS as the SL. Some of these substrates have features such as flexibility, biocompatibility, and biodegradability.

To test whether alloys other than EGaIn can be fabricated to MPC, we used LM with higher melting point. We sonicated an alloy that melts at 47°C (Sn 8.30, Pb 22.60, Bi 44.70, Cd 5.30, In 19.10) into LMPs and utilize partial transfer to fabricate the MPC on PET. At room temperature, the LM within the MPC is in solid state. The MPC possesses excellent flexibility; after bending for 1,000 cycles, the conductivity remains the same (Figure S7A). MPC can thus be a general approach for making flexible conductors by combining LM with a variety of polymers, as long as the melting pointing of the metal alloy is within the working range of polymers.

We can pattern the MPC into any complex 2D geometry using handwriting (Figure S7B), screen printing, or microfluidic patterning (Figure 3H). To achieve rapid fabrication of patterns, we used screen printing to make a batch of nine integrated circuits, each circuit controlling an array of light-emitting diode (LED) (Figure 3E). Each circuit is highly supple and can undergo repeated bending, twisting, and stretching without compromising the function of any of its components (Figure 3G and Video S1). We achieved such circuit array within 10 s, which suggested that an estimated number of 2,000 circuits can be obtained within 1 hour when taking the casting and peeling off process into account. Comparing with direct ink-jet printing of LM, which requires LM 60 mg/cm^2 (the patterns are usually 100 μm in thickness) (Wang et al., 2015), the MPC fabricated by screen printing is unprecedented in minimizing the amount of metal, only several milligrams per square centimeter (depending on the concentration of inks, Figure 3B). The LMPs on the mesh can be easily washed by ethanol. After the printing, we usually wash the mesh using ethanol and collect such washed LMPs. After centrifugation, LMPs can be recycled. The thickness of the MPC can be controlled by the concentration of the LMP inks (Figure 3C). We achieved MPC patterns on an ultrathin membrane (30 μm) (Figure S7D). We successfully achieved multi-layered circuits by stacking MPC patterned on pieces of PDMS (Figure 3D). This approach may allow us to ultimately make stretchable displays (Figures 3F and S7C).

We used microfluidic patterning method to obtain ultra-fine interconnects. Briefly, we used a blade to scrap the LMP inks into the microfluidic channels (Figure 3H). When scraping the LMP ink, the LMPs will not be broken by blades because they are in a solution form (dispersed in solvent and cannot be sintered). After evaporation of the solvents, we used sticky PDMS as the SL to retain half of the MPC in the microfluidic channels. We achieved a minimum trace width of 15 μm on PDMS (Figure 3I) using this method (the discrete ink residues by the wide lines caused by the surface tension of the solvents may be improved by increasing the concentration of the LMP inks or by adding some surfactants). Microfluidic patterning method is also suitable for converting a Printed circuit board (PCB) into flexible and stretchable circuit. Using a PCB as a convex mold (Figure 3J), we can replicate a concave microfluidic network, which allows the filling of LMP inks (Figures 3K and 3L). Our MPC patterning strategies perfectly meet the requirements of the industrial standard PCB, where the minimum trace width is ~70 μm. Compared with conventional patterning strategies of LM, the patterning of the MPC could be much more flexible, economic, and extremely high in yield.

MPC Sensors and Wearable Glove Keyboards

We fabricated strain sensors for motion capture using the MPC patterns (entire transfer, and PDMS as the SL) (Figure 4A). We attached these sensors onto the knuckles of a glove, and monitored the motion of the fingers in real time (Video S2). The detected signals have good repeatability when we bent and straightened the finger with high frequency (Figure 4B). When slowly and evenly bending and straightening different fingers, the signals showed a good linear relationship with time, which demonstrated that our sensors have high motion resolution to reflect different degrees of bending of fingers (Figure 4C).

Based on the high repeatability of the MPC (Figure 2F), we developed a wearable QWERTY keyboard on a pair of gloves using an array of sensors. Wearable keyboards can dramatically improve the productivity of work; this improvement can accelerate the process of converting ideas to texts. We use MPC sensors to

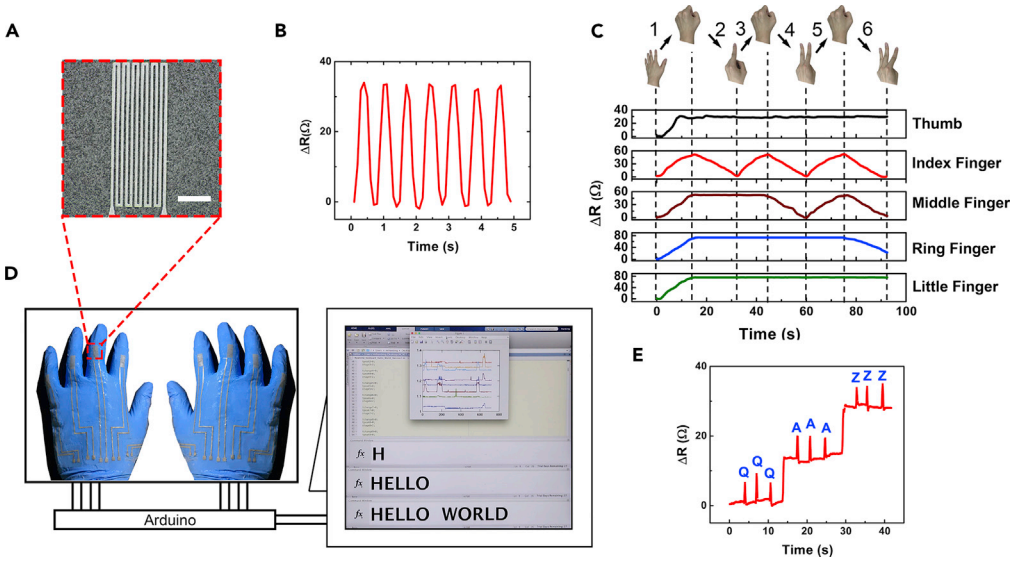

Figure 4. Fully Printed MPC Strain Sensors for Motion Monitoring and a Wearable Glove Keyboard

(A) Photograph of the strain sensor. Scale bar, 2 mm.

(B) Electrical signals from finger bending and straightening with high frequency.

(C) Motion monitoring of five fingers with slow bending and straightening: 1. making a fist; 2. straightening index finger; 3. bending index finger; 4. straightening two fingers; 5. bending two fingers; 6. straightening three fingers.

(D) Using a wearable glove keyboard to input the phrase "HELLO WORLD."

(E) An example showing left little finger typing the letters Q, A, and Z.

See also Figure S8, and Video S2.

convert mechanical signals into electrical ones and use Arduino and MATLAB to process electrical signals, which mainly comprise peak recognition, cliff recognition, and the elimination of the interference peak caused by neighboring fingers when typing. Our keyboard suits the traditional typing style where each finger is responsible for typing three letters. For example, the left little finger is responsible for the input of Q, A, and Z (Figure 4E). The three levels of resistance signals represent three different bending degrees of the finger, whereas the peaks represent the tapping movements. We typed the phrase "HELLO WORLD" using this wearable glove keyboard (Figures 4D and S8). The robustness of the MPC under stretch ensures that a real device as complex as the keyboard can function properly. Since each sensor has to accurately differentiate between at least six modes of stretch, the entire device with 10 sensors will have to accommodate 60 parameters repetitively. MPC can thus be instrumental in developing a series of wearable devices.

MPC for Live-Cell Electroporation

To explore the biocompatibility and biodegradability of the MPC, we fabricated the MPC cast by PDMS to culture human umbilical vascular epithelial cells (HUVECs) and human aortic fibroblasts (HAFs). After a 7-day incubation in the cell culture medium, the cells showed good viability (Figure S9), which demonstrated that MPC is safe to cells. We found that the surface of MPC is slightly degraded (Figures 5B and 5C) without compromising its conductivity (Figure S10A), whereas the control group exposed to cell culture medium alone showed no degradation (Figure S10B). We speculate that the metabolic wastes from cells, such as CO_2, reduced the pH around the MPC to partially dissolve the LM. This experiment indicates that neither the MPC itself nor its dissolvable components (such as gallium ion and indium ion) are toxic to mammalian cells.

To further explore the biomedical potential of MPC, we designed comb-like MPC electrodes and performed electroporation to introduce exogenous genes into live cells. The controlled introduction of exogenous materials into live cells using stretchable devices is a potentially useful, but a poorly explored area. To verify the excellent stretchability of MPC electrodes, we exerted tensile cycle for 100 times to the MPC electrode (Figure 5A) before electroporation, using gold electrodes of the same geometry as a control. The gold electrodes lost their conductivity owing to the formation of cracks after the first tensile cycle (Figure S10C). After adhesion of HAFs on the MPC electrodes, we delivered DNA plasmid encoding GFP

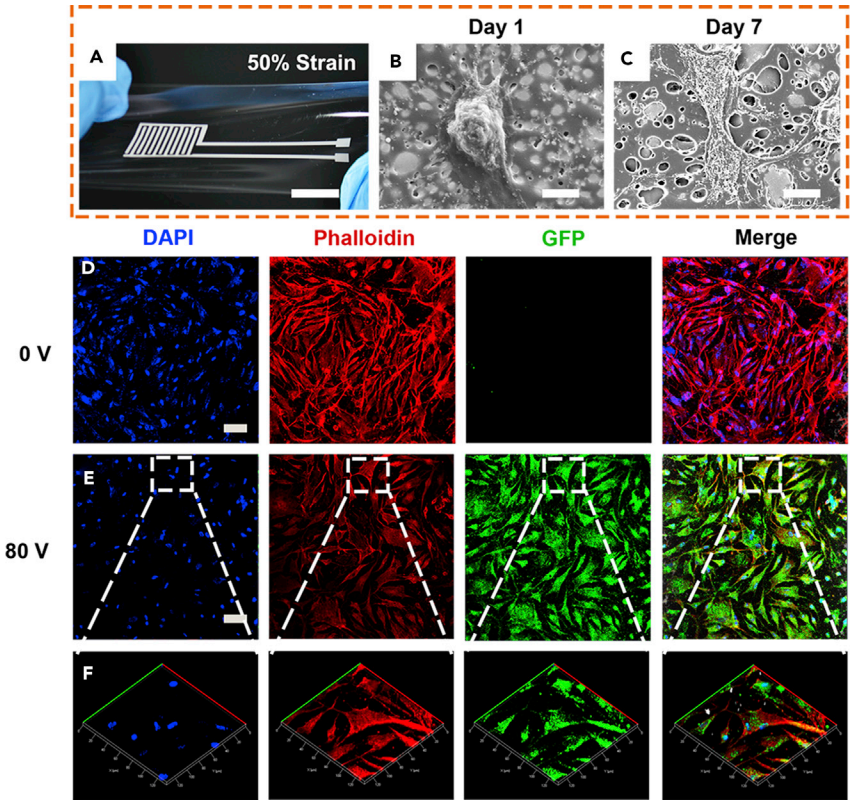

Figure 5. Cell Culture and Electroporation Using MPC Electrode

(A–E) (A) Photograph showing the MPC electrode under stretch, scale bar, 8 mm. Scanning electron microscopic characterization of HUVEC on the surface of MPC on (B) day 1 and (C) day 7, scale bar, 10 μm. Fluorescent cytoskeleton staining of fibroblasts on the MPC (D) without and (E) with electroporation. Scale bar, 50 μm.

(F) 3D reconstruction of fibroblasts on the MPC treated by electroporation.

See also Figures S9–S11.

into HAF by electroporation. We stimulated cells with a voltage of 80 V five times by exerting a square wave. After a 24-hr incubation, the HAFs on the electrodes (Figures 5E and 5F) and between the electrodes (Figure S11) successfully realized GFP expression, with 95% of cells showing green fluorescence, whereas there was no green fluorescence in the control group (Figure 5D). Thus MPC can function as completely biocompatible, biofunctional, and stretchable electronics.

DISCUSSION

In this work, we reported a straightforward MPC patterning strategy. Through the printing, casting, and peeling off steps, we could easily achieve any 2D pattern of MPC on most substrates in different thickness with high resolution, high efficiency, and low cost, which cannot be achieved by reported strategies in LM, because in these studies, the performances of LM are constrained by limited substrates (Zheng et al., 2014) (few substrates can be wetted by LM), poor resolution (Jeong et al., 2015a, 2015b) (limited by surface tension and the stencil), inability to achieve arbitrary patterns (Kubo et al., 2010; Zhu et al., 2013) (for example, injecting LM into microfluidic channels or hollow wires), high LM consumption caused by low efficiency and utilizations (Wang et al., 2015; Lin et al., 2015; Boley et al., 2015; Ren et al., 2016; Mohammed and Kramer, 2017; Jeong et al., 2015b) (most of the LMs are wasted on stencils or not as the conductive part), or undesirable sintering of the LMPs (Mohammed and Kramer, 2017) (stress caused by deformation can sinter the LMPs in regions where conductive patterns are not desirable). Because MPC patterns allow exposed LMs on the surface of solid substrates (instead of completely buried within polymers), electronic components could be easily mounted. Compared with stretchable silver ink (Matsuhisa et al., 2017), our MPCs have not only better performances but also low cost, because the price of gallium is about one-quarter of that of silver (silver: ~ US $530 per kilogram, gallium: ~ US $150 per kilogram, indium: ~ US $180 per

kilogram, 2018) (as conductors, gallium and indium in high purity are not necessary), not to mention the expensive processing of the microstructured silver. Our MPC patterning method meets the minimum trace width requirements of the commercial PCB, and its low cost and high yields will make broad applications of the LM-based electronic devices possible.

We can combine the benefits of both metals and polymers. We may use functional polymers such as shape memory polymers, self-healing polymers, and biodegradable polymers to cast the LMPs to form thousands of new functional MPCs in desirable temperature.

Our MPC also paves a brand new avenue for the implantable electronic devices. Based on the excellent stretchability and biocompatibility of our MPC, stretchable patches can be designed for highly active organs, such as the heart and joints. For example, in a myocardial infarction model, we intend to fabricate a biodegradable cardiac patch patterned by MPC electrodes to enhance the conductivity of myocardial cells and monitor the electrophysiological signals simultaneously.

The ease of fabrication and high level of biocompatibility will make MPC useful for wearable electronics, implantable devices, soft robotics, future fabrics, virtual/augmented reality, flexible display, artificial organs, brain-computer interface, and wherever biocompatible, soft electronics is necessary.

METHODS

All methods can be found in the accompanying Transparent Methods supplemental file.

SUPPLEMENTAL INFORMATION

Supplemental Information includes Transparent Methods, 11 figures, 1 table, and 2 videos and can be found with this article online at https://doi.org/10.1016/j.isci.2018.05.013.

ACKNOWLEDGMENTS

We thank Zewen Wei and Deyao Zhao for their great help in electroporation. We thank the Ministry of Science and Technology of China (2013YQ190467), Chinese Academy of Sciences (XDA09030305), and the National Natural Science Foundation of China (81361140345, 51373043, and 21535001) for financial support.

AUTHOR CONTRIBUTIONS

X.J. conceived and supervised this project. L.T. designed, fabricated, and characterized materials and devices with the help of L.M., and S.Y., L.T., S.C., and Z.H. carried out cell experiments. L.Z. and X.S. performed the calculation and simulation of the MPC. H.M. coded the virtual keyboard. L.T., S.C., and X.J. wrote the manuscript. All authors discussed the results and commented on the manuscript.

DECLARATION OF INTERESTS

The authors declare that they have no competing interests.

Received: March 27, 2018
Revised: April 30, 2018
Accepted: May 1, 2018
Published: June 14, 2018

REFERENCES

Boley, J.W., White, E.L., and Kramer, R.K. (2015). Mechanically sintered gallium-indium nanoparticles. Adv. Mater. *27*, 2355–2360.

Chortos, A., Liu, J., and Bao, Z. (2016). Pursuing prosthetic electronic skin. Nat. Mater. *15*, 937–950.

Dickey, M.D. (2014). Emerging applications of liquid metals featuring surface oxides. ACS Appl. Mater. Interaces *6*, 18369–18379.

Dickey, M.D. (2017). Stretchable and soft electronics using liquid metals. Adv. Mater. *29*. 1606425. https://doi.org/10.1002/adma.201606425.

Gao, H.L., Xu, L., Long, F., Pan, Z., Du, Y.X., Lu, Y., Ge, J., and Yu, S.H. (2014). Macroscopic free-standing hierarchical 3D architectures assembled from silver nanowires by ice templating. Angew. Chem. Int. Ed. *53*, 4561–4566.

Jeong, J.W., McCall, J.G., Shin, G., Zhang, Y., Al-Hasani, R., Kim, M., Li, S., Sim, J.Y., Jang, K.I., Shi, Y., et al. (2015a). Wireless optofluidic systems for programmable in vivo pharmacology and optogenetics. Cell *162*, 662–674.

Jeong, S.H., Hjort, K., and Wu, Z. (2015b). Tape transfer atomization patterning of liquid alloys for microfluidic stretchable wireless power transfer. Sci. Rep. *5*, 8419.

Kang, S., Murphy, R.K.J., Hwang, S., Lee, S.M., Harburg, D.V., Krueger, N.A., Shin, J., Gamble, P., Cheng, H., Yu, S., et al. (2016). Bioresorbable silicon electronic sensors for the brain. Nature *530*, 71–76.

Kazem, N., Hellebrekers, T., and Majidi, C. (2017). Soft multifunctional composites and emulsions with liquid metals. Adv. Mater. *29*, 1–14.

Kim, D.H., Song, J., Choi, W.M., Kim, H.S., Kim, R.H., Liu, Z., Huang, Y.Y., Hwang, K.C., Zhang, Y., and Rogers, J.A. (2008). Materials and noncoplanar mesh designs for integrated circuits with linear elastic responses to extreme mechanical deformations. Proc. Natl. Acad. Sci. USA *105*, 18675–18680.

Kim, D.H., Lu, N., Ma, R., Kim, Y.S., Kim, R.H., Wang, S., Wu, J., Won, S.M., Tao, H., Islam, A., et al. (2011). Epidermal electronics. Science *333*, 838–843.

Kim, Y., Zhu, J., Yeom, B., Di Prima, M., Su, X., Kim, J.G., Yoo, S.J., Uher, C., and Kotov, N.A. (2013). Stretchable nanoparticle conductors with self-organized conductive pathways. Nature *500*, 59–63.

Kubo, M., Li, X., Kim, C., Hashimoto, M., Wiley, B.J., Ham, D., and Whitesides, G.M. (2010). Stretchable microfluidic radiofrequency antennas. Adv. Mater. *22*, 2749–2752.

Lin, Y., Cooper, C., Wang, M., Adams, J.J., Genzer, J., and Dickey, M.D. (2015). Handwritten, soft circuit boards and antennas using liquid metal nanoparticles. Small *11*, 6397–6403.

Lipomi, D.J., Vosgueritchian, M., Tee, B.C.K., Hellstrom, S.L., Lee, J.A., Fox, C.H., and Bao, Z. (2011). Skin-like pressure and strain sensors based on transparent elastic films of carbon nanotubes. Nat. Nanotechnol. *6*, 788–792.

Liu, J., Fu, T.M., Cheng, Z., Hong, G., Zhou, T., Jin, L., Duvvuri, M., Jiang, Z., Kruskal, P., Xie, C., et al. (2015). Syringe-injectable electronics. Nat. Nanotechnol. *10*, 629–636.

Lou, Z., Chen, S., Wang, L., Shi, R., Li, L., Jiang, K., Chen, D., and Shen, G. (2017). Ultrasensitive and ultra flexible E-skins with dual functionalities for wearable electronics. Nano Energy *38*, 28–35.

Lu, Y., Hu, Q., Lin, Y., Pacardo, D.B., Wang, C., Sun, W., Ligler, F.S., Dickey, M.D., and Gu, Z. (2015). Transformable liquid-metal nanomedicine. Nat. Commun. *6*, 10066.

Matsuhisa, N., Inoue, D., Zalar, P., Jin, H., Matsuba, Y., Itoh, A., Yokota, T., Hashizume, D., and Someya, T. (2017). Printable elastic conductors by in situ formation of silver nanoparticles from silver flakes. Nat. Mater. *5*, 1–8.

Mohammed, M.G., and Kramer, R. (2017). All-printed flexible and stretchable electronics. Adv. Mater. *29*. 1604965. https://doi.org/10.1002/adma.201604965.

Oh, J.Y., Rondeau-gagné, S., Chiu, Y., Chortos, A., Lissel, F., Wang, G.N., Schroeder, B.C., Kurosawa, T., Lopez, J., Katsumata, T., et al. (2016). Intrinsically stretchable and healable semiconducting polymer for organic transistors. Nature *539*, 411–415.

Qi, D., Liu, Z., Liu, Y., Leow, W.R., Zhu, B., Yang, H., Yu, J., Wang, W., Wang, H., Yin, S., et al. (2015). Suspended wavy graphene microribbons for highly stretchable microsupercapacitors. Adv. Mater. *27*, 5559–5566.

Ren, L., Zhuang, J., Casillas, G., Feng, H., Liu, Y., Xu, X., Liu, Y., Chen, J., Du, Y., Jiang, L., et al. (2016). Nanodroplets for stretchable superconducting circuits. Adv. Funct. Mater. *26*, 8111–8118.

Sekitani, T., Nakajima, H., Maeda, H., Fukushima, T., Aida, T., Hata, K., and Someya, T. (2009). Stretchable active-matrix organic light-emitting diode display using printable elastic conductors. Nat. Mater. *8*, 494–499.

Sun, J., Xianyu, Y., and Jiang, X. (2014). Point-of-care biochemical assays using gold Nanoparticle-implemented Microfluidics. Chem. Soc. Rev. *43*, 6239–6253.

Tang, Y., Gong, S., Chen, Y., Yap, L.W., and Cheng, W. (2014). Manufacturable conducting rubber ambers and stretchable conductors from copper nanowire aerogel monoliths. ACS Nano. *8*, 5707–5714.

Wang, Q., Yu, Y., Yang, J., and Liu, J. (2015). Fast fabrication of flexible functional circuits based on liquid metal dual-trans printing. Adv. Mater. *27*, 7109–7116.

Zheng, Y., He, Z.Z., Yang, J., and Liu, J. (2014). Personal electronics printing via tapping mode composite liquid metal ink delivery and adhesion mechanism. Sci. Rep. *4*, 4588.

Zhu, S., So, J.H., Mays, R., Desai, S., Barnes, W.R., Pourdeyhimi, B., and Dickey, M.D. (2013). Ultrastretchable fibers with metallic conductivity using a liquid metal alloy core. Adv. Funct. Mater. *23*, 2308–2314.

ISCI, Volume *4*

Supplemental Information

Printable Metal-Polymer Conductors for Highly Stretchable Bio-Devices

Lixue Tang, Shiyu Cheng, Luyao Zhang, Hanbing Mi, Lei Mou, Shuaijian Yang, Zhiwei Huang, Xinghua Shi, and Xingyu Jiang

SUPPLEMENTAL FIGURES

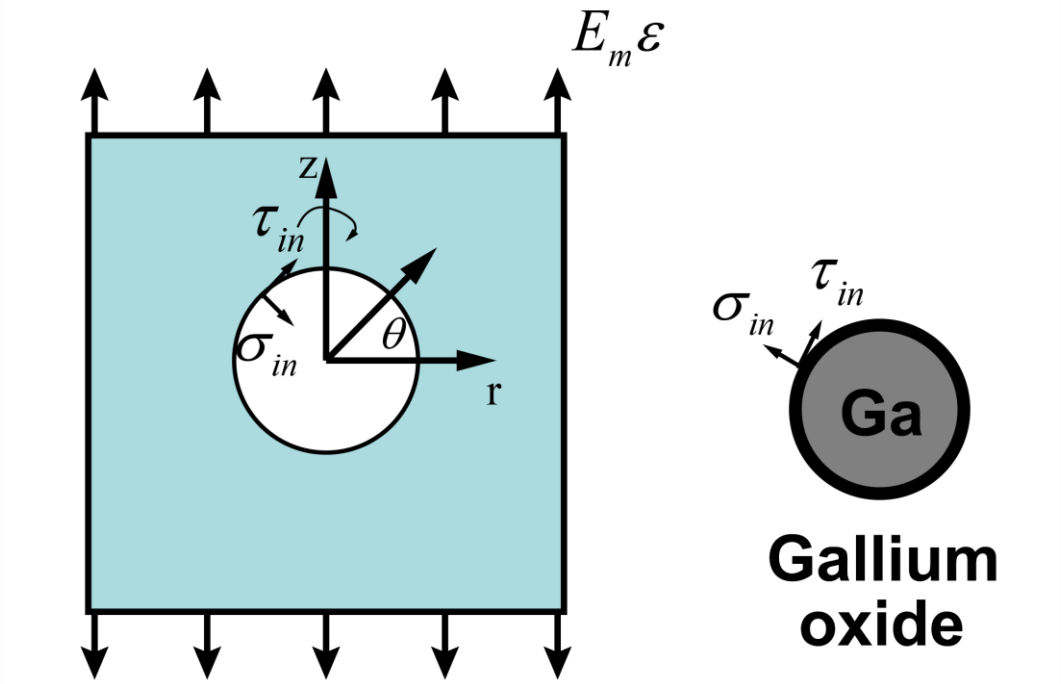

Figure S1. The diagram of uniaxial loading, related to Figure 1. The stress components at the interface of PDMS matrix and gallium oxide shell is σ_{in} and τ_{in}.

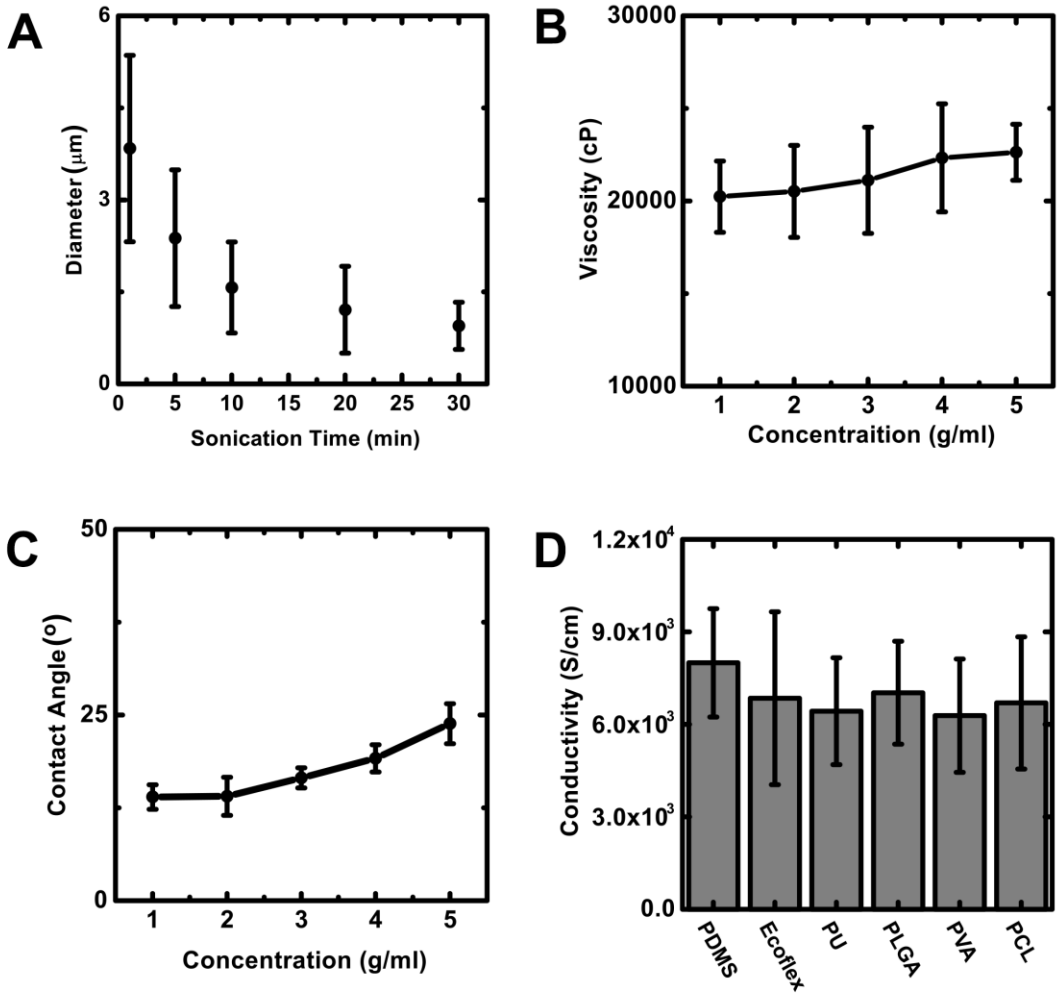

Figure S2. Characterization of the LMPs ink, **related to Figure 1.** (**A**) Average diameter of LM particles as a function of sonication time. (**B**) The viscosity of the ink as a function of the concentrations of the ink. (**C**) The contact angle between the LMPs inks with different concentrations and the PET film. (**D**) Conductivity of MPC cast by different polymers. Data are expressed as mean ±SD.

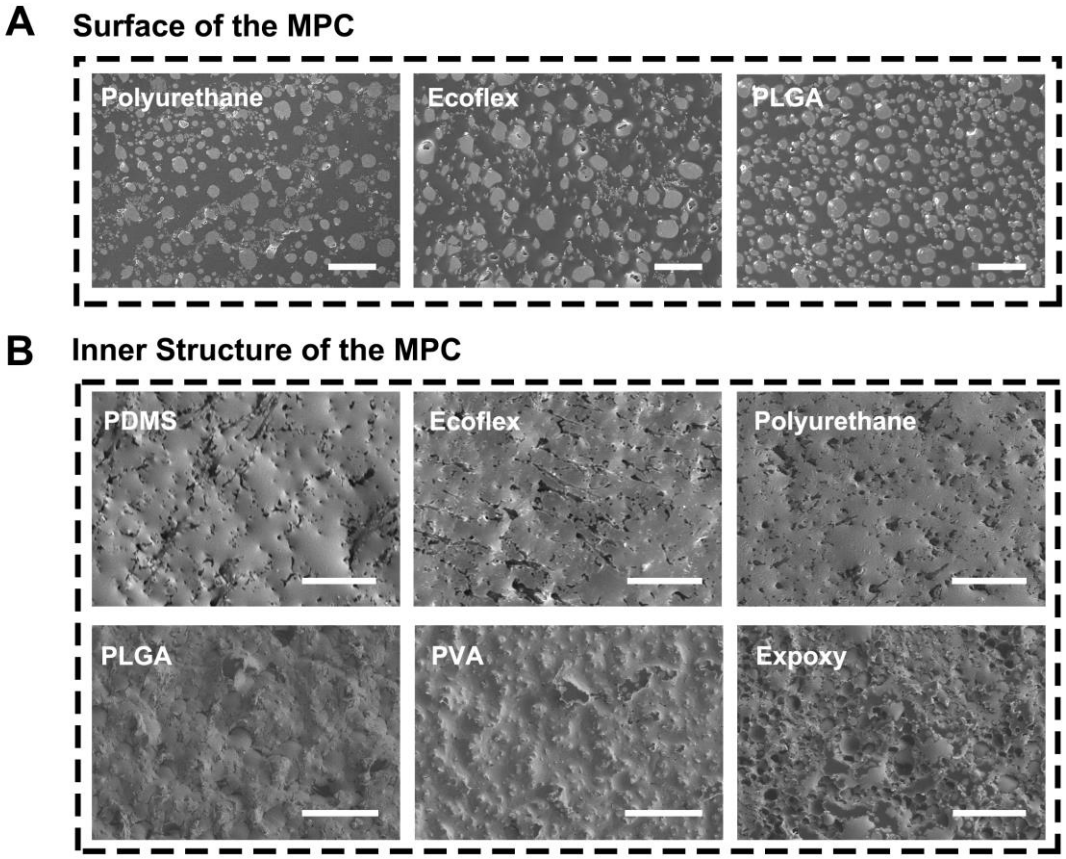

Figure S3. Characterization of the MPC cast by different polymers, **related to Figure 2.** (**A**) The surface appearances of MPC cast by polyurethane, Ecoflex, and PLGA, and it present an appearance of LM islands dispersing in the sea of polymer. Scale bar, 20 μm. (**B**) The pattern surfaces in partial transfer which represent the inner structure of the MPC; they all have continuous metallic phase. Scale bar, 20 μm.

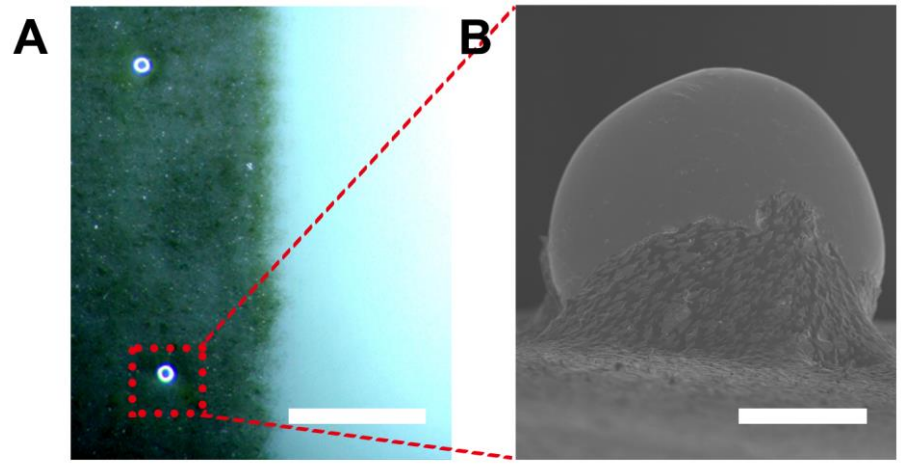

Figure S4. Characterization of the MPC after the stretch cycle, related to Figure 2. (A) Optical image of the MPC after the stretch cycle, several liquid metal droplets are squeezed out from the MPC, scale bar 500 μm. **(B)** SEM image of the squeezed liquid metal droplet. Scale bar 30 μm.

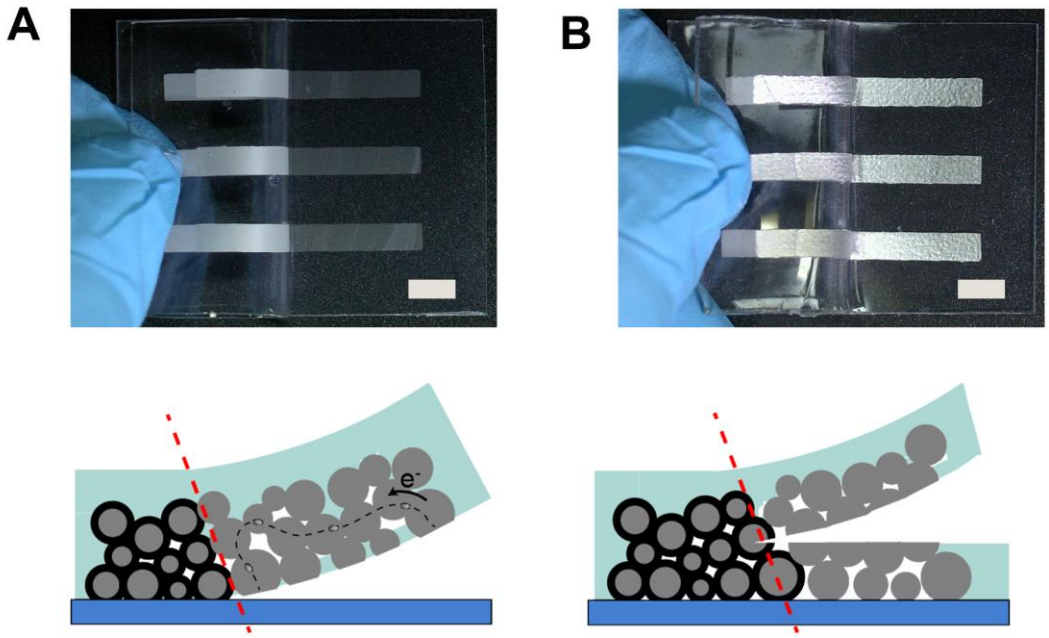

Figure S5. Entire transfer and partial transfer, **related to Figure 3.** (**A**) Entire transfer of the MPC patterns to the SL (PDMS), leaving only oxide on the IPL (PET

film). (**B**) Partial transfer of the MPC patterns, and both of the IPL and SL have integrated MPC pattern. Scale bar 10 mm.

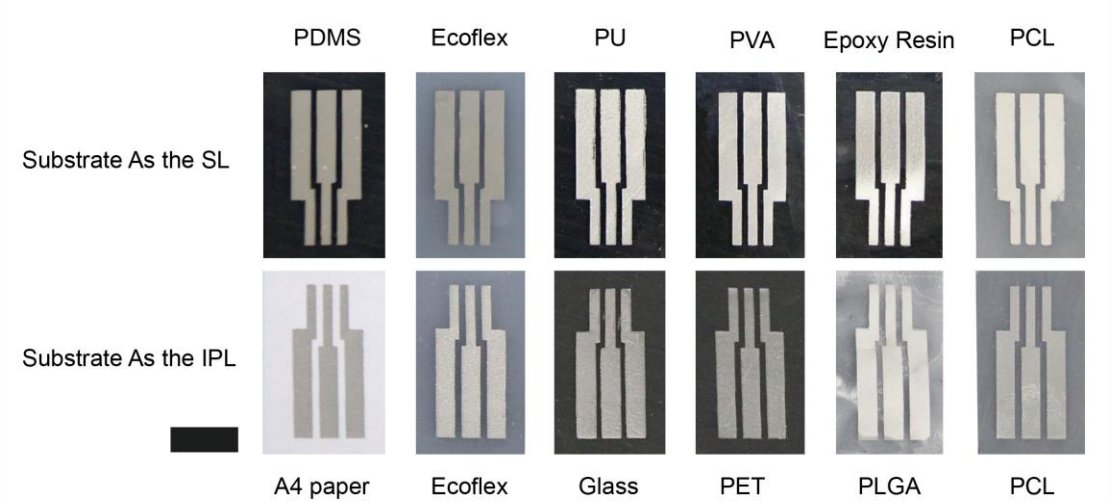

Figure S6. MPC transfer to different substrates, related to Figure 3. Scale bar, 10 mm.

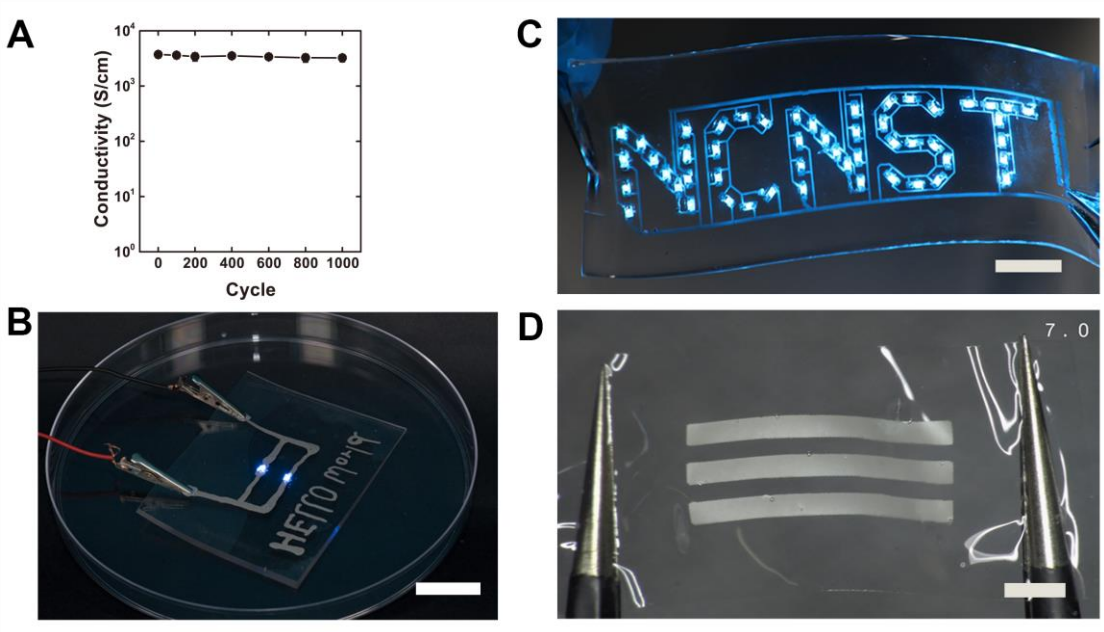

Figure S7. MPC patterns as interconnects, related to Figure 3. (**A**) Conductivity changes with the bending for 1,000 cycles. (**B**) We use handwriting method to fabricate a flexible and stretchable LED circuit on the PDMS substrate. Scale bar, 15

mm. (**C**) A simple LED display interconnected by MPC on PDMS substrate, scale bar, 20 mm. (**D**) MPC patterns fabricated on ultrathin PDMS film (30 μm). Scale bar, 4 mm.

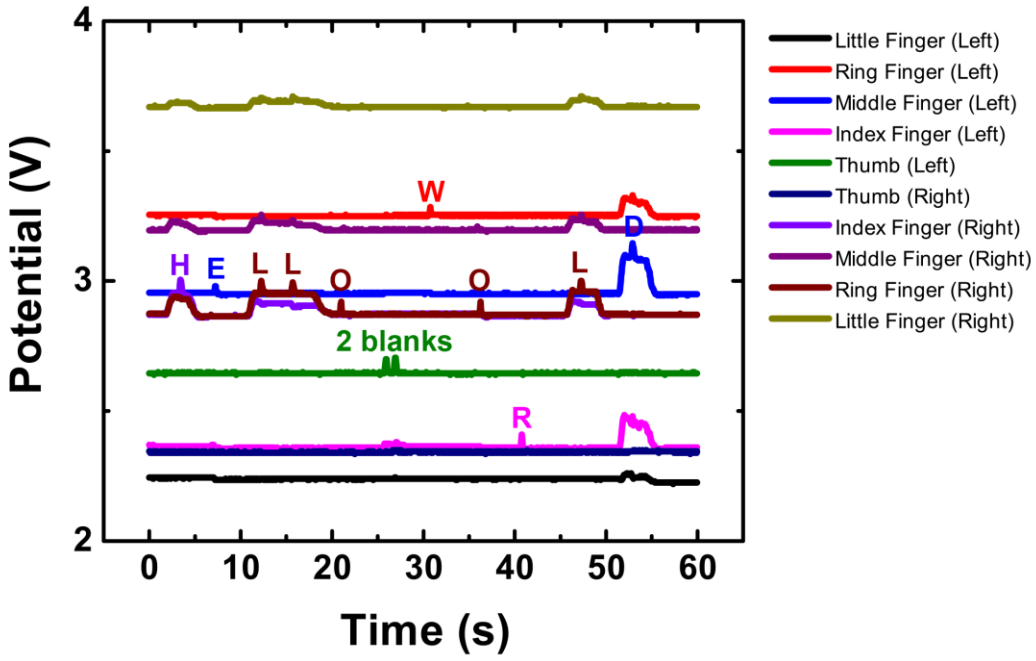

Figure S8. Potentials across the strain sensors versus time when we use the virtual keyboard to type "HELLO WORLD", related to Figure 4.

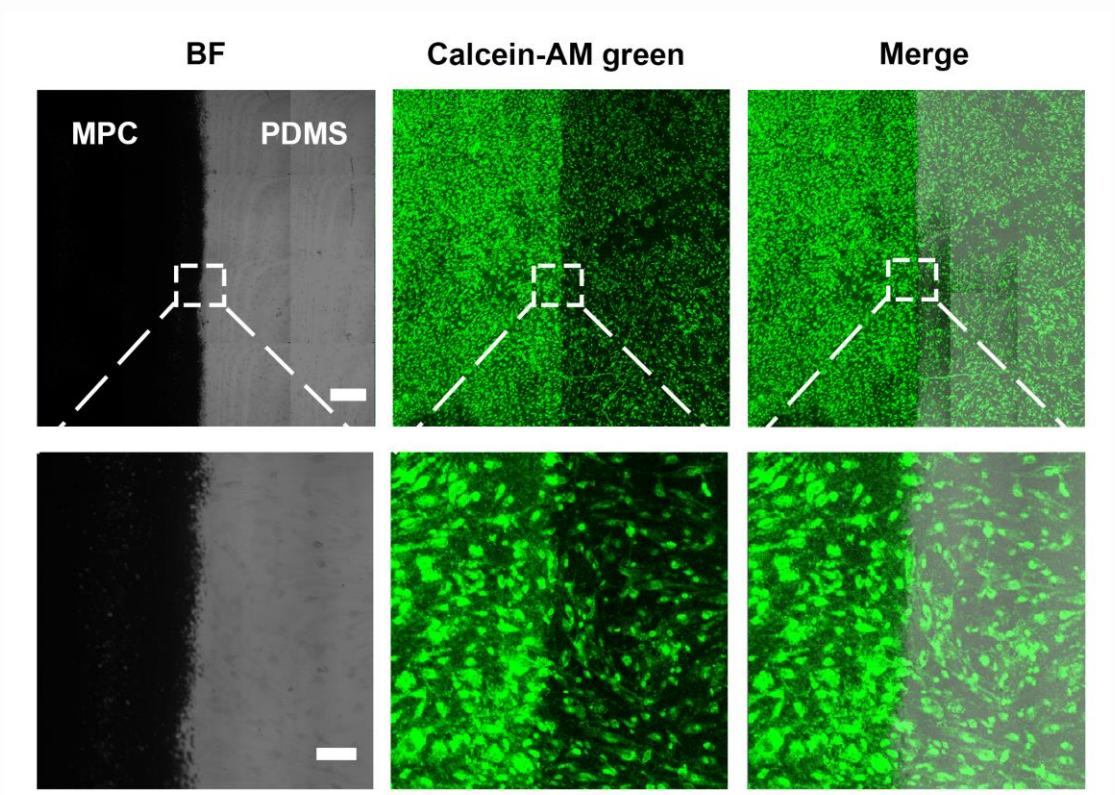

Figure S9. Viability test of the HUVECs on the MPC-PDMS interface after 7 days, related to Figure 5. Cells are stained by Calcein-AM green (Invitrogen, US), Scale bar, (top) 400 μm, (bottom) 100 μm.

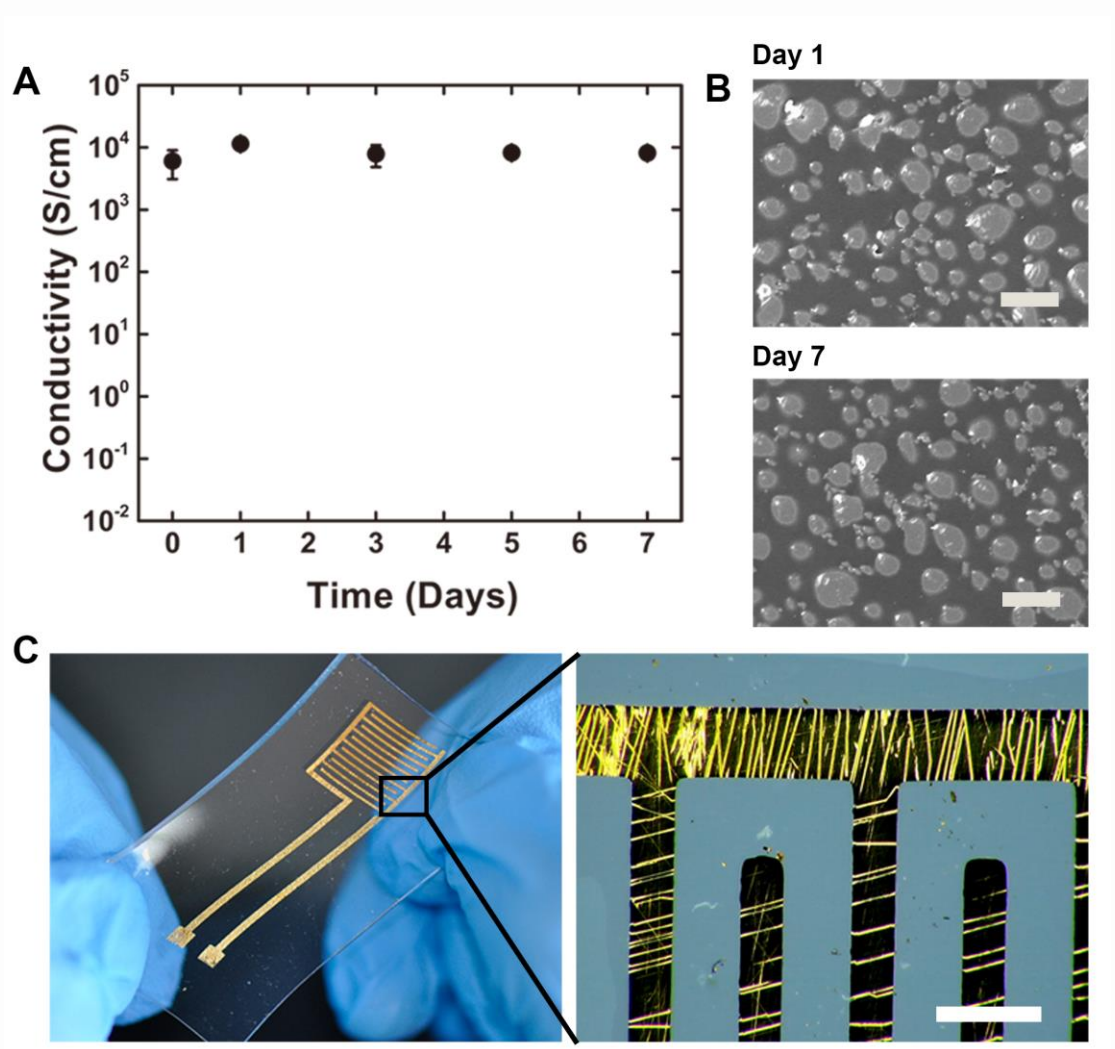

Figure S10. Tolerance of the MPC and the gold electrode, related to Figure 5. (**A, B**) Degradation exploration of the MPC. (**A**) Conductivity of the MPC dependence on culturing time. (**B**) SEM characterization of the surface of MPC electrodes exposed in DMEM. Scale bar, 10 μm. (**C**) The gold electrode on the PDMS substrates lost its conductivity after the tensile cycle due to the forming of cracks. Scale bar, 500 μm. Data are expressed as mean ±SD

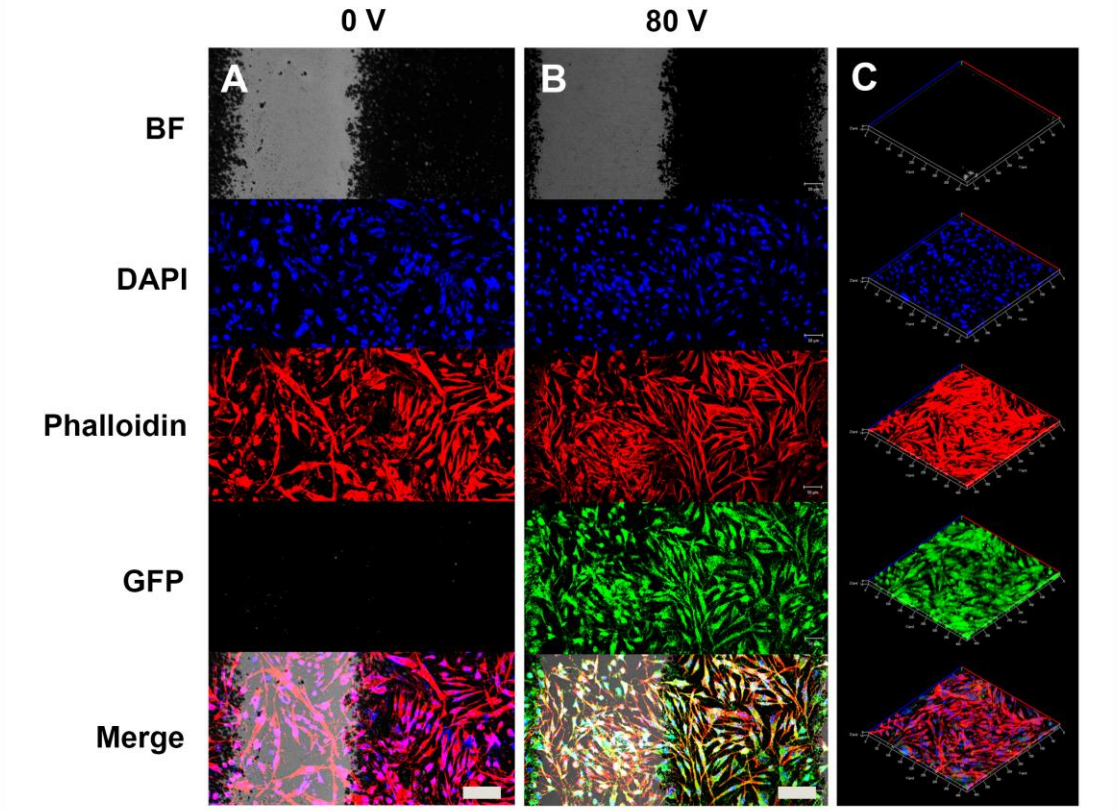

Figure S11. GFP plasmid delivery in Fibroblasts, related to Figure 5. A, B, Fluorescent cytoskeleton staining of fibroblasts on and adjacent to the MPC (**A**) without and (**B**) with electroporation. Scale bar, 100 μm. **(C)** 3D distribution of fibroblasts on the MPC treated by electroporation. The nucleus (blue) and F-actin (red) are stained by Hoechst 33342 and Alexa Fluor 568-labelled phalloidin, respectively.

SUPPLEMENTAL TABLES

Table S1. Typical value of parameters we used in this study, related to Figure 1.

The Young's modulus and Poisson's ratio of Gallium Oxide [a]	E_s=8 GPa μ_s=0.3	The Young's modulus and Poisson's ratio of PDMS	E_m=1.2 MPa μ_m=0.5
The yield stress of Gallium Oxide [a]	σ_y=200 MPa	The thickness of the PDMS	h =50 μm
The radius of droplets	**R**=3 μm	The thickness of Gallium oxide film [b]	t =0.5 nm
The typical curvature of the PDMS film	κ=1 mm^{-1}		

[a] (Dickey et al., 2008)

[b] (Boley et al., 2015)

TRANSPARENT METHODS

Mechanical Calculation. We obtained micro particles of gallium alloy through sonication. The surface of these droplets will form an oxidation layer (Lin et al., 2015; Boley et al., 2015). The thickness of the oxide layer is about 0.5 nm (Boley et al., 2015). This thin oxide layer will keep the shape of the droplets and make it behave like an elastic material (Boley et al., 2015; Lawrenz et al., 2015). When the film experience a large enough stress, it will yield and flow readily (Lawrenz et al., 2015). According to the data of Dickey et al.'s previous research (Dickey et al., 2008), the Young's modulus (E) and the yield stress (σ_y) of the oxidation layer are estimated to be 8 GPa and 200 MPa respectively.

To prove the stress during stripping can effectively break the oxide layer of LMPs embedded in elastomers, we performed theoretical calculation. We analyze the stress of liquid metal particles on the bending part (Fig. 1a). The model can be simplified as a gallium particle embedded in a PDMS (polydimethylsiloxane) matrix. When we peeled the PDMS film off the glass matrix, the liquid metal particle patterns will be conductive. Based on this, we will give a theory explanation of this phenomenon.

When we peel the PDMS film off a substrate like PET, the film will have a curvature. The gallium droplets are at the bottom of the PDMS. So they will suffer a large stress and the oxide layer of the gallium droplets will yield.

According to the bending theory, the stain at the bottom of the PDMS can be written as

$$\varepsilon = \frac{\kappa h}{2} \quad (1)$$

In which, h is the thickness of the PDMS and κ is the curvature radius of the PDMS. We will calculate the relation of the stress of gallium droplet and the PDMS strain ε. As shown in fig. S1, the PDMS matrix is assumed as an infinite solid and the gallium droplet with a thin oxide layer is assumed as a thin walled sphere with a radius *R* and a thickness *t*. Far from the sphere, the matrix is subjected to a tensile stress $\sigma_z = E_m\varepsilon$, with all other stress componets zero. The stress field of PDMS matrix σ'_{ij} is

$$\sigma'_r = \frac{B}{2} + \left[A - \frac{3}{2}C\right]\frac{1}{r^3} + \frac{D}{2r^5} + \frac{1}{2}\left[B - 9\frac{C}{r^3} + 3\frac{D}{r^5}\right]\cos 2\theta \quad (2)$$

$$\sigma'_\theta = \frac{B}{2} - \frac{A}{2r^3} - \frac{D}{8r^5} - \left(\frac{B}{2} + \frac{7D}{8r^5}\right)\cos 2\theta \quad (3)$$

$$\sigma'_\varphi = -\frac{A}{2r^3} - \frac{3D}{8r^5} - \frac{5D}{8r^5}\cos 2\theta \quad (4)$$

$$\tau'_{r\theta} = \left(-\frac{B}{2} - \frac{3C}{2r^3} + \frac{D}{r^5}\right)\sin 2\theta \quad (5)$$

And in which, *A*, *B*, *C*, *D* are constants which are determined by the boundary conditions. Then the stress filed of the oxide layer of the gallium droplet σ_{ij} can be written as

$$\sigma_\theta = \frac{R}{t}\left(H + I\cos 2\theta\right) \quad (6)$$

$$\sigma_\varphi = \frac{R}{t}\left[\sigma_a - H + \left(\sigma_b - I\right)\cos 2\theta\right] \quad (7)$$

Where *H*, *I* and σ_b are constants. And the boundary condition is at $r \to \infty$,

$$\sigma'_r = \frac{E_m\varepsilon}{2} + \frac{E_m\varepsilon}{2}\cos 2\theta \quad , \quad \tau'_{r\theta} = -\frac{E_m\varepsilon}{2}\sin 2\theta \quad (8)$$

And finally, we can obtain the maximum Tresca's equivalent stress of the oxide layer is

$$\sigma_{\max} = \frac{5RE_m\varepsilon}{2t} \quad (9)$$

The typical value of parameters we used in this study are listed in table S1. Substituting the value in table 1 in the Equation (9), we obtain

$$\sigma_{\max} = 4500 \text{ MPa}$$

And this value is great larger than the yield stress of gallium oxide (about 200 MPa). So the oxide layer of the gallium droplet will yield.

Preparation of the low-melting metal particle inks. 1 g, 1.5 g, 2g, 2.5 g, 3 g, 4 g, and 5 g EGaIn (Gallium Indium eutectic, 99.99%, Sigma-Aldrich) was added into 5 mL centrifuge tube filled with 1 mL n-Decyl alcohol (98%, MACKLIN, China), respectively and sonicated by a sonicator (Scientz, Scientz-IID). For screen printing, we sonicated the EGaIn for 1 min with the power of 300 W. For microfluidic patterning, 5 min with 300 W is required.

We also adopted alloy with melting point 47 °C (Sn 8.30, Pb 22.60, Bi 44.70, Cd 5.30, In 19.10, Taobao, China) to prepare the low-melting metal particle inks. 2.5 g alloy was added to 1 mL n-Decyl alcohol (98%, MACKLIN, China). We heated the alloy in an oven at 80 °C for 10 min to melt the alloy and sonicated the melting alloy for 1 min with the power of 300 W.

Screen printing of the LMPs ink. The printing of liquid metal particle was realized by a screen printing equipment (Taobao, China). We used the liquid metal particle ink to print desired patterns on various substrates including PET, PCL, PLGA, PDMS films, A4 paper, and glass with 200 mesh screen printing plates.

Microfluidic patterning of the LMPs ink. The microstructures are obtain by soft lithography. Briefly, we used silicon wafer or printed circuit boards (PCB) as the master molds. To obtain silicon wafer as the master wafer, we followed standard photolithography. Master fabrication for the microfluidic channels begins with spin coating negative photoresists (SU8 2035, MicroChem Corp., US) on a silicon wafer at 1200 rpm for 30 s (100 μm thick). After baking the photoresist at 95 °C for 5 min, the wafer was exposed to UV light for 90 s through a mask. After baking the wafer at 95 °C for 10 min, we immersed the wafer into a developer (SU8 developer, MicroChem Corp, US.) and washed it for 5 min.

We also use the PCB (Jiekecengfeng Corp., China) as the master wafer. The thickness of the copper film is 150 μm. We cast a layer of PDMS onto the master mold. After baking in an oven at 80 °C for 40 min, we removed the PDMS replica from master. We spread LM particle inks onto the patterned PDMS. Before the evaporation of the solvent, we filled the microfluidic channel with EGaIn particle ink using a blade or squeegee, and excess ink was scraped off the substrate.

The fabrication of MPC by casting and peeling. After evaporation of the solvent, we used various polymers for casting on the patterned LMPs. We dissolved poly (carprolactone) (PCL, Mn=80000 g/mol, Sigma-Aldrich, US) pellets in dimethylformamide (DMF, ThermoFisher Scientific, US) and CH_2Cl_2 (Aladdin, China) with a ratio of 1:3 (w/w) at 5 wt% to prepare the PCL solution. We prepared the 5 wt% poly (vinyl alcohol) (PVA) (1795, Aladdin, China) solution (w/w) by dissolving PVA in ultrapure water (Milli-Q Reference, MERCK, France) in water bath at 95 °C for 1 hour. We dissolved poly (DL-lactide-co-glycolide) (PLGA 75:25, Mw=114 kDa, Lakeshore Biomaterials, US) particles in acetone/DMF with a ratio of 2:1 (w/w) at 5 wt% to prepare the PLGA solution. We prepared the PDMS prepolymer by mixing base and curing agent with a ratio of 10:1, 15:1, 20:1, 25:1, 30:1, and 35:1 (w/w). We prepared the Ecoflex prepolymer by mixing part A and part B with a ratio of 1:1 (w/w). We prepared the epoxy sealant prepolymer (epoxy sealant, Ausbond, US) by mixing part A and part B with a ratio of 5:4 (w/w). We prepared the polyurethane (PU) (polyurethane sealant, Ausbond, US) prepolymer by mixing part A and part B with a ratio of 1:1 (w/w). These prepolymers were thoroughly mixed and degassed in a mixer (AR-100, THINKY, Japan).

We cast polymer solutions or prepolymers onto the LMPs patterns. These cast polymer solutions were placed in a chemical hood in room temperature for 24 h to volatile solvents. While the cast PDMS, PU, and epoxy resin prepolymers were placed in 80 ^{o}C oven for 40 min or in room temperature for 12 hours.

After curing, these polymer films were peeled off from the substrates. Thus conductive MPC on different polymer substrates were obtained either on IPL or SL. To obtain MPC patterns on the PDMS ultrathin film (30 μm), we spin-coated the PDMS at 4500 r for 20 s after the casting process.

Particles and MPC characterization. Inks (2.5 g/mL for 1 min) for Scanning Electron Microscopy (SEM, S4800, Hitachi, Japan) characterizations were fabricated by sonicating EGaIn for 1 min, 5 min, 10 min, 20 min, and 30 min, respectively. We deposited 100 μL suspension on conductive tape via micropipette (Eppendorf, Germany) and allowed them to dry in 80 ^{o}C oven for 10 min. MPC for SEM characterizations were prepared by screen printing using different polymers as SL (PDMS, Ecoflex, PLGA, PVA, PCL, PU, and epoxy resin).

The LM dissolved MPC for SEM characterizations were fabricated by immersing the MPC patterns (2.5 g/mL) on 0.1 M sulfuric acid for 10 h. We use the LM dissolved MPC for the thickness measurements. Briefly, we cut the sample with a blade and characterized the cross section of the sample using SEM.

Measurement of the liquid metal consumptions and transfer amount of the MPC. We used screen printing method to print liquid metal particles (2.5 g/mL) on PET films as a shape of a strip (3*30 mm). After the evaporation of solution in an oven at 80 ^{o}C for 10 min, we cast PDMS of different ratio (10:1, 15:1, 20:1, 25:1, and 30:1) on different PET films, respectively. The PDMS films were peeling from PET films after curing in 80 ^{o}C for 40 min. We weighed these PET films using a precision balance (AL104, METTLER TOLEDO, Swizerland) before printing, after printing, after evaporation, and after peeling off, respectively.

Tensile test. Samples for stretching test were prepared by screen printing inks with concentration of 1 g/ml, 2 g/ml, 3 g/ml, 4 g/ml, and 5 g/ml, respectively. We made the MPC into a strip shape (800 μm in width and 4 cm in length) using PET as the IPL and Ecoflex as the SL. The MPC strips were connected with a 100 Ω resistance and mounted on a homemade frame. We measured resistance of the MPC using multimeter (8846A, FLUKE, US) when they were gradually stretched to 500% strain.

Cycling test. Samples for stretching cycling test were prepared by screen printing EGaIn inks with concentration of 2.5 g/ml. Samples for bending cycling test were prepared by screen printing 47 ^{o}C low melting alloy particle inks with concentration of 2.5 g/ml. We made the MPC into a strip shape (800 μm in width and 2 cm in length) using PET as the IPL and PDMS (10:1) as the SL. We performed the stretching cycling test for 10,000 cycles using a dynamic mechanic analysis (DMA Q800, TA Instruments, US) under a strain rate of 100% /min with maximum strain of

50%. We performed the bending tests on dynamic mechanic analysis under a strain rate of 100% /min with a displacement of 1 cm for 1,000 cycles

Circuits assembly. To assembly a functional circuits, we first used a pipette to add 2 μL EGaIn onto each contact pad of interconnects. Subsequently, we gently rubbed EGaIn into the surface of electronic components to wet their pins and connected electronic components with the touch pads. Finally, a layer of elastomer was cast to encapsulate the circuits.

Fabrication and characterization of the strains sensors and virtual keyboard. We printed EGaIn LMPs ink (2.5 g/mL) on PET films by screen printing as serpentine shapes with the width of 200 μm. After solvent evaporation at 80 ^{o}C for 10 min, we spin-coated the PDMS (10:1) at 1000 r for 20 s on the LMPs patterns. . After curing at 80 ^{o}C for 30 min, the PDMS films with serpentine MPC (strain sensors) were carefully peeled off from PET films. We used silica adhesive (3145 RTV, Dow Corning, US) to attach strain sensors on a glove to monitor the motion of different fingers by capturing resistance change.

We wore the strain sensors-mounted glove to monitor motions of fingers. The strain sensors were connected to electrochemical workstation (1040C, CH Instruments, US). We tested the resistant changes of the sensors by using the technique amperometric i-t curve at potential 0.001 V.

The virtual keyboards were achieved by connecting the glove to Arduino (MEGA 2560, ITALY), and processed signals using MATLAB.

Cell culture, staining and characterization. Samples for cell experiments were prepared by screen printing inks with concentration of 2.5 g/ml. We made the MPC using PET as the IPL and PDMS (10:1) as the SL. Before cell culture, we sterilized all the samples by radiation with a cobalt radiation device (Co 5 60, 10-130 Gymin-1, Peking University, China). The MPC was incubated with fibronectin solution (50 μg/ml) for 6 h at room temperature to promote the adhesion of cells. We seeded human umbilical vein endothelial cells (HUVECs, ATCC, US) and human aortic fibroblasts (Science Cell, US) on the surface of the MPC, and culture them in DMEM supplemented with 10% fetal bovine serum (5% CO_2, 37 ^{o}C) for 7 days. HUVECs were stained with live/dead kit (Invitrogen, US) for cell viability test. Briefly, we fixed cells with 4% paraformaldehyde aqueous solution for 10 min. Subsequently, we stained the cells with the dyes at a concentration of 1 μg/mL for 20 min, and removed excess dyes by 3 times rinsing the cells with phosphate buffered saline (PBS). (Invitrogen, US) We stained the nucleus with Hoechst 33342 (Invitrogen, US) at a concentration of 1 μL/mL for 5 min, and removed excess dyes by 3 times rinsing the cells with PBS. We stained the F-actin with Alexa Fluor 568-labelled phalloidin (Invitrogen, US) at a concentration of 200 units/mL for 20 min, and removed excess dyes by 5 times rinsing the cells with PBS. The fluorescent images of cells was taken by laser scanning confocal microscopy (LSM 710, Zeiss, Germany). Before SEM characterization, we fixed cells with 4% paraformaldehyde aqueous solution for 30

min and dehydrated the sample with ethanol at the concentrations of 50%, 75%, and 100% for 10 min, sequentially.

Electroporation. We printed the MPC electrodes for electroporation with 2.5 g/mL EGaIn LMPs, using PDMS (10:1) as the SL and PET as the IPL. We deposited 100 nm thick gold on the surface of PDMS by evaporation (Ohmiker-50B, Cello Technology Corporation, Taiwan) to fabricate gold electrodes as a control group. Human aortic fibroblasts were used to verify the electroporation of green fluorescent protein (GFP, RiboBio, China). We incubated the MPC electrodes with the fibronectin plasma solution (50 μg/ml) for 6 h at room temperature to promote adhesion of cells. Subsequently, fibroblasts were delivered on the MPC electrode (PDMS as the substrates) and cultured for 24 h. We washed the sample 3 times before electroporation and immersed the surface of the electrodes in GFP solution at a concentration of 40 μg/ml. We applied 5 electrical pulses using an electroporator by exerting a square wave pulse (Electro Square Porator ™ ECM 830, BTX, USA). The voltage is 80 V, the pulse duration is 100 μs, and the pulse interval is 1 s. After culturing for 24 h, we stained the cells as above-mentioned and used confocal microscopy to image the cells.

SUPPLEMENTAL REFERENCES

Lawrenz, F.; Lange, P.; Severin, N.; Rabe, J. P.; Helm, C. A.; Block, S. Morphology, Mechanical Stability, and Protective Properties of Ultrathin Gallium Oxide Coatings. (2015). *Langmuir* 31, 5836–5842.

Dickey, B. M. D.; Chiechi, R. C.; Larsen, R. J.; Weiss, E. A.; Weitz, D. A.; Whitesides, G. M. Eutectic Gallium-Indium (EGaIn): A Liquid Metal Alloy for the Formation of Stable Structures in Microchannels at Room Temperature. (2008). *Adv. Funct. Mater.* 18, 1097-1104.